

Westfälische Wilhelms-Universität Münster
Fachbereich Physik
Institut für Kernphysik

Bachelorarbeit

Design of a Tabletop Spectrometer following the MAC-E-Filter Principle

Maik Schneider

Matrikel Nr.: 370659

05. September 2014

1. Gutachter: Prof. Dr. Weinheimer
2. Gutachter: Prof. Dr. Wessels

Contents

1. Introduction	3
1.1. The discovery of the neutrino and beta decay	3
1.2. Kinematic search for the neutrino mass in tritium β -decay	3
2. MAC-E-filter principle	4
2.1. Energy resolution and transmission function	6
2.2. Preliminary setup	8
3. Electric potential and magnetic field calculations and particle tracking	11
3.1. FEMM	11
3.1.1. Preprocessor	11
3.1.2. Postprocessor	13
3.2. Particle tracking	14
4. Design of a tabletop MAC-E-filter	16
4.1. Magnetic setup	16
4.2. Electrostatic setup	18
4.3. Particle tracks	20
5. Conclusion and outlook	24
A. Electrode voltages	26
References	27

1. Introduction

In the standard model 3 neutrinos (tau-,muon- and electron neutrino) exist. They belong into the Lepton family as massless, electrical neutral particles with 1/2-spin. But the observation of oscillation of the weak eigenstates of neutrinos showed that the neutrino possesses a non-vanishing mass. Today this is one of the biggest trails towards physics beyond the standard model. But the absolute mass of the neutrinos has yet to be found. Since it is an important parameter not only in particle physics but also in cosmology and astrophysics, a lot of experiments searching for the neutrino mass have been conducted. While cosmological experiments have set good boundaries on the neutrino mass, their results are model-dependent and so a kinematic approach to determine the neutrino mass is necessary[D⁺13].

1.1. The discovery of the neutrino and beta decay

In 1914 J. Chadwick experimentally found that the β -spectrum was continuous[Cha14], contrary to the expected discrete spectrum which had already been found in α - and γ -decays, which was in agreement with the new picture of a quantized nucleus. At first this even lead to the assumption that energy- and momentum-conservation could be violated in the β -decay. But calorimetric measurements, conducted by C.D. Ellis and W.A. Wooster[EW27], showed that energy was still conserved. Around 1930 Wolfgang Pauli suggested the existence of a third neutral particle, which took away the missing momentum, breaking with the picture of a two-body process, which the radioactive disintegration was thought of up till then[Pau64].

In the β^- -decay a neutron decays into a proton, emitting an electron and an anti-electron neutrino. Taking place inside an atom it is described by the formula

$$(A, Z) \rightarrow (A, Z + 1)^+ + e^- + \bar{\nu}_e + Q. \quad (1)$$

(A, Z) and $(A, Z + 1)$ describe the mother and daughter nuclei, respectively, and Q denotes the energy that is set free in the decay process.

Enrico Fermi was the one to succeed in giving a theoretical description of a β -decay with a third partner in 1934[Fer34]. To distinguish the new particle from the much heavier, but also neutral neutron it was called neutrino. The experimental discovery of the neutrino took until 1956, when F. Reines and C.L. Cowan could observe the inverse β -decay[RC59],

$$\bar{\nu}_e + p \rightarrow n + e^+. \quad (2)$$

The reason to why it is so challenging to detect the neutrino mass, is that the neutrino does not interact via the electro-magnetic nor the strong interaction and since its mass is very small, the only way to detect a neutrino at all is via the weak interaction, e.g. through β -decay.

1.2. Kinematic search for the neutrino mass in tritium β -decay

In the endpoint region of the β -spectrum the imprint of the neutrino mass is the strongest. A shift of the highest electron energy and moreover a change in the shape of the spectrum, corresponding to the neutrino mass, should be visible if the neutrino mass is nonzero, as seen in figure 1.

KATRIN (KArlsruhe TRItium Neutrino experiment) is an experiment currently looking for

the change in the spectrum via the MAC-E-filter principle, succeeding the Mainz and Troitsk MAC-E-filter experiments, which have set a boundary for the neutrino mass of $2.2 \text{ eV}/c^2$ [K⁺05] and $2.5 \text{ eV}/c^2$ [Lob03] respectively. KATRIN aims at a precision of $0.2 \text{ eV}/c^2$ at 90% C.L. and can detect a neutrino mass down to $0.35 \text{ eV}/c^2$.

Unfortunately the endpoint region only contains a very small fraction of decays. Therefore a β -emitter needs a low half-life to ensure a suitable count rate. In the aforementioned experiments, tritium was chosen as the β -emitter, with a half life of $T_{1/2} = 12.3 \text{ a}$ and an endpoint energy of $E_0 = 18.6 \text{ keV}$. The endpoint energy is also an important factor for the election of a β -emitter discussed in chapter 2.

This work covers the design of a tabletop MAC-E-filter. Optimizing and testing of the design will be done via, simulation of the electron trajectory.

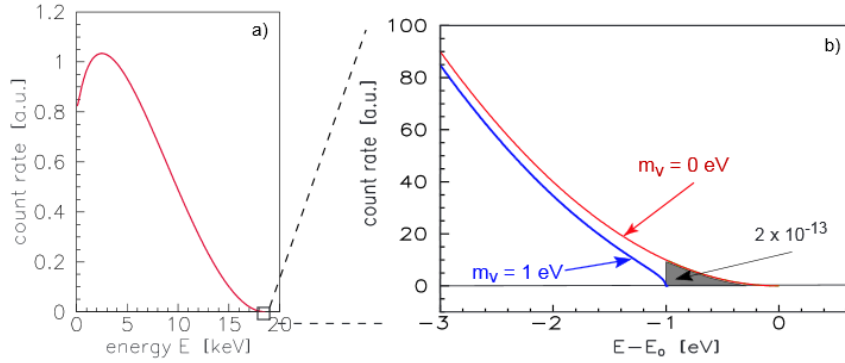


Figure 1: electron energy spectrum of the tritium beta-decay(a) with a close up of the endpoint region(b). The picture in the endpoint region shows the analytical spectrum(blue line, $m_\nu = 0 \text{ eV}$) and the expected shape for a spectrum with a non-vanishing neutrino mass(red line, $m_\nu = 1 \text{ eV}$). Taken from the KATRIN design report[KAT04]

2. MAC-E-filter principle

A general problem in using electric retardation is that they only analyze energy parallel to the electric field. The magnetic adiabatic collimation with an electrostatic filter(short MAC-E-filter) is a working principle for a spectrometer aiming to allow the analysis of the total energy of a particle, by combining electric retardation and an inhomogeneous magnetic guiding field[P⁺92].

As shown in figure 2 the electron is placed inside a static magnetic field, which guides it from the source to the detector. The field strength is maximal at the source and detector and drops over several magnitudes in between, reaching its minimum at the point of maximal retardation, which is called the analyzing plane.

An electron emitted into the MAC-E-filter with a starting energy E_{start} , under an angle $\theta = \angle(\vec{B}, \vec{p})$ between its momentum \vec{p} and the magnetic field \vec{B} , performs a cyclotron motion around the field line in which the perpendicular energy

$$E_\perp = E_{start} \sin^2(\theta) \quad (3)$$

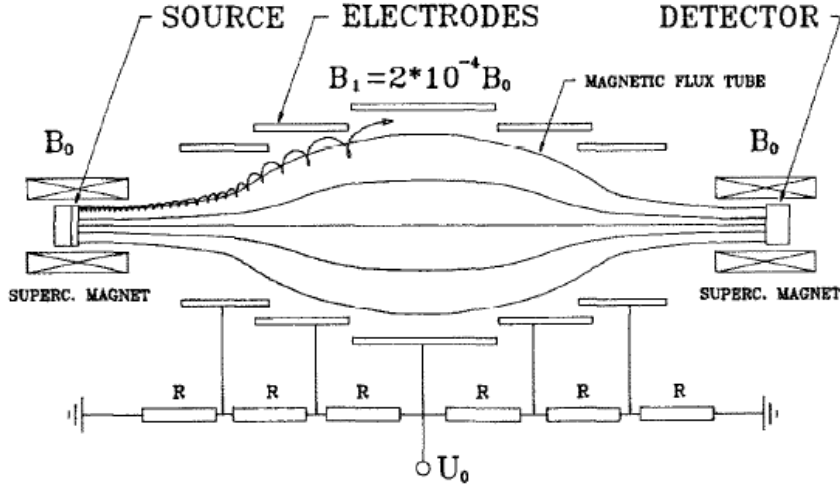


Figure 2: Cross section of a MAC-E-Filter setup. The source is located in the left solenoid at a magnetic field strength of B_0 . At the analyzing plane the magnetic field decreases to B_1 , transforming most of the perpendicular energy of the electrons into parallel energy, which is analyzed by the electric potential of the ringelectrodes. Figure taken from [P⁺92]

is stored, thus creating an orbital magnetic moment

$$\mu = \frac{q}{2m} |\vec{l}| = \frac{E_{\perp}}{B}, \quad (4)$$

where \vec{l} is the angular momentum. Through the gradient of the magnetic field a force parallel to the field lines is applied, and since the energy is conserved in a static magnetic field the energy perpendicular to the field lines E_{\perp} is converted into parallel energy E_{\parallel} . Another requirement of the MAC-E-filter is the adiabatic movement of the electron, which means that the change of the magnetic field in one cyclotron motion is sufficiently low¹. If this requirement is fulfilled, the product of the absolute value of the magnetic moment and the relativistic lorentz factor γ are a constant of motion. Since electrons from tritium β -decay only reach $\gamma \approx 1.04$, it can be said that

$$\mu = \frac{E_{\perp}}{B} = \text{const.} \quad (6)$$

Which immediately allows to determine the change of the perpendicular energy and the angle θ between a starting point p_i and an endpoint p_f :

$$E_{\perp,f} = E_{\perp,i} \frac{B_f}{B_i}. \quad (7)$$

¹A mathematical expression of the adiabatic criterium is

$$\left| \frac{1}{B} \frac{dB}{dt} \right| \ll \omega_{cyc} = \frac{qB}{m} \quad (8)$$

2.1. Energy resolution and transmission function

Now the energy resolution can be found by looking at the extreme case of an electron starting with a 90° pitch angle. The initial energy is completely stored in the perpendicular direction ($E_{start} = E_{\perp,i}$). Assuming the electron passed from maximal to minimal magnetic field strength, transforming as much of the energy into parallel energy as possible, the remaining perpendicular energy is

$$\Delta E = E_{start} \frac{B_{min}}{B_{max}}. \quad (8)$$

Theoretically the energy resolution only depends on the inhomogeneity of the field. But there is another practical reason which limits the energy resolution of a MAC-E-filter. The magnetic flux,

$$\Phi = \int B dA, \quad (9)$$

is a conserved quantity, i.e. at the point of the lowest field strength the spectrometer radius needs to be in proportion to the ratio from the maximal field strength to the lowest field strength and the size of the source area. The source area itself also cannot be arbitrarily small, since only about 10^{-13} of all decay electrons reach the detector and a suitable count rate has to be guaranteed. Here the count rate becomes the same magnitude as the estimated background rate, so the resolution is also limited by the cross-section area in the analyzing plane that is practically realizable.

To be transmitted through the MAC-E-filter, an electron needs to fulfill the requirement

$$E_{\parallel}(\vec{r}) > qU(\vec{r}) \quad \forall \vec{r}. \quad (10)$$

Therefore the MAC-E-filter is a high-pass filter for electrons. Using equation (3) we can express this requirement in dependence of the angle to the magnetic field

$$E_{\parallel,ana} = E_{start} \left(1 - \sin^2 \theta_{start} \frac{B_{ana}}{B_{source}} \right) > qU_{ana}, \quad (11)$$

where $E_{\parallel,ana}$, B_{ana} is the parallel energy and the magnetic field in the analyzing plane respectively and B_{source} is the magnetic field strength at the source.

Assuming $E_{start} > qU_{ana}$, equation (11) can define a cone of emission in which all electrons fulfill the requirement to pass the MAC-E-filter:

$$\theta \leq \theta_{max} = \arcsin \left(\sqrt{\frac{E_{start} - qU_0}{E_{start}} \frac{B_{src}}{B_{ana}}} \right). \quad (12)$$

Given the angular acceptance of the spectrometer of $\Delta\Omega = 2\pi$, the fraction of electrons that pass the filter is described by the transmission function:

$$T(E_{start}, qU_0) = \begin{cases} 0 & \text{for } E_{start} < qU_0, \\ 1 - \sqrt{1 - \frac{E_{start} - qU_0}{E_{start}} \frac{B_{src}}{B_{ana}}} & \text{for } E_{start} \left(1 - \frac{B_{ana}}{B_{src}} \right) \leq qU_0 \leq E_{start}, \\ 1 & \text{for } qU_0 \leq E_{start} \left(1 - \frac{B_{ana}}{B_{src}} \right). \end{cases} \quad (13)$$

However this is only correct if the magnetic field strength at the source is the maximum field strength in the setup. Using a field strength higher than the source strength creates a magnetic mirror, which reflects all electrons with a larger angle than

$$\theta_{start}^{max} = \arcsin \left(\sqrt{\frac{B_{src}}{B_{max}}} \right). \quad (14)$$

A magnet that produces this kind of field is called pinch magnet.

Cutting off electrons with higher angles is a method to reduce the effects of inelastic scattering inside the source and thus reduce systematic errors.

If there is a field strength $B_{max} > B_{src}$ in the setup, the transmission function normalized to one becomes:

$$T(E_{start}, qU_0) = \begin{cases} 0 & \text{for } E_{start} < qU_0, \\ \frac{1 - \sqrt{1 - \frac{E_{start} - qU_0}{E_{start}} \frac{B_{src}}{B_{ana}}}}{1 - \sqrt{1 - \frac{B_{src}}{B_{max}}}} & \text{for } qU_0 \leq E_{start} \leq qU_0 \frac{B_{max}}{B_{max} - B_{ana}}, \\ 1 & \text{for } qU_0 \leq E_{start} \left(1 - \frac{B_{ana}}{B_{src}} \right). \end{cases} \quad (15)$$

Figure 3 shows a transmission function for a MAC-E-filter with a pinch magnet.

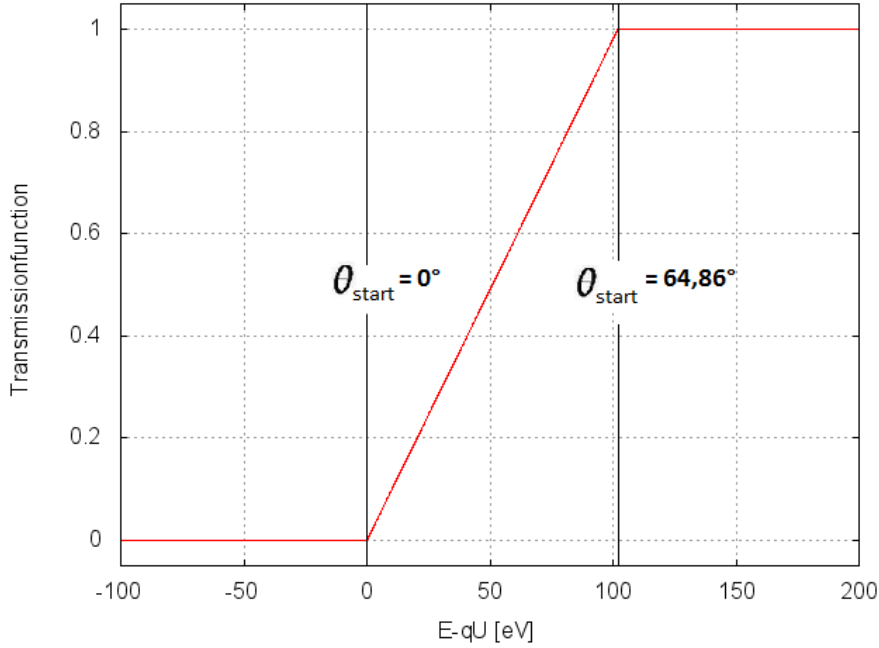


Figure 3: Normalized transmissionfunction $T(qU_0, E_{start})$ plottet after equation 15. The maximum angle ($\theta = 64.86^\circ$) and energy resolution ($\Delta E = 102$ eV) are calculated for the field strengths in the setup explained in chapter 4.1.

For different retarding potentials the electrons that pass the filter are counted. The spectrum that is measured with a MAC-E-filter is an integrated one. By differentiating the measured spectrum it is possible to compare the results with the analytical spectrum, which leads to the mass of the neutrino.

2.2. Preliminary setup

The preliminary idea to create a tabletop MAC-E-filter came from E.W.Otten. His original magnetic and electrostatic setup are schematically pictured in figure 4 and 5 respectively. These pictures are taken from the program FEMM (finite element method magnetics[Mee10]), which will be explained in detail in chapter 3.1.

The geometry of the experiment is placed inside a cylindrical vacuum chamber and is symmetrical around the z-axis and x-axis, which allows to observe the whole setup in a 2D-cross section, from the symmetry axis ($r = 0$) to the outer wall ($r = 115$ mm) and from the analyzing plane ($z = 0$ mm) to the top cover ($z = 110$ mm).

In contrast to the setup from the Troitsk, Mainz and KATRIN-experiments, here the magnetic field is produced by a single permanent magnet instead of solenoids. The magnetic flux flows from the north to the south pole of the magnet, where the β -emitter and detector are respectively placed.

To increase the inhomogeneity of the field, a magnetic screen was implemented in the setup. It is made of soft iron and absorbs the magnetic field lines, weakening the field strength behind the screen and shifting the analyzing plane closer to the center of the setup. The inner radius of the screen is $r_i = 45$ mm and it's 2.5 mm thick.

Electrode	Voltage [V]
1 + 8	5600
2 + 9	3060
3 + 10	1800
4 + 11	1140
5 + 12	690
6 + 13	410
7 + 14	260

Table 1: retardation voltages of the electrodes in the preliminary setup

Another difference to the in chapter 2 mentioned MAC-E-filter setup, is that the field lines do not exit the magnet parallel to the symmetry-axis. The opening angle only amounts to $\alpha_{cl} \approx 70^\circ$ clockwise, of course the solid opening angle is still $\Delta\Omega = 2\pi$, with a counterclockwise opening angle of $\alpha_{ccl} \approx 130^\circ$. But since the electric field exits normal to the surface electrons with the same starting angle starting clockwise and counterclockwise experience a different field in the beginning. If this results in a difference of the adiabatic motion and with it a difference in the transmission function is analyzed in chapter 4.3, since this phenomenon is also occurring in the final setup.

The electric field in this setup is produced by several toroidal electrodes, as well as the outer walls, the central magnet and the magnetic screen, which are all used as electrodes for the electric field.

The toroid electrodes are placed on both sides of the central field line to form the electric field parallel to the central field line, therefore opposing electrodes are also put on the same voltage. Since the cyclotron radius increases along the way to the analyzing plane due to the decreasing magnetic field strength, the distance of the electrodes to the central field line increase along the way. Table 1 lists the retarding potentials of the electrodes as they are numbered in the

figure from left to right.

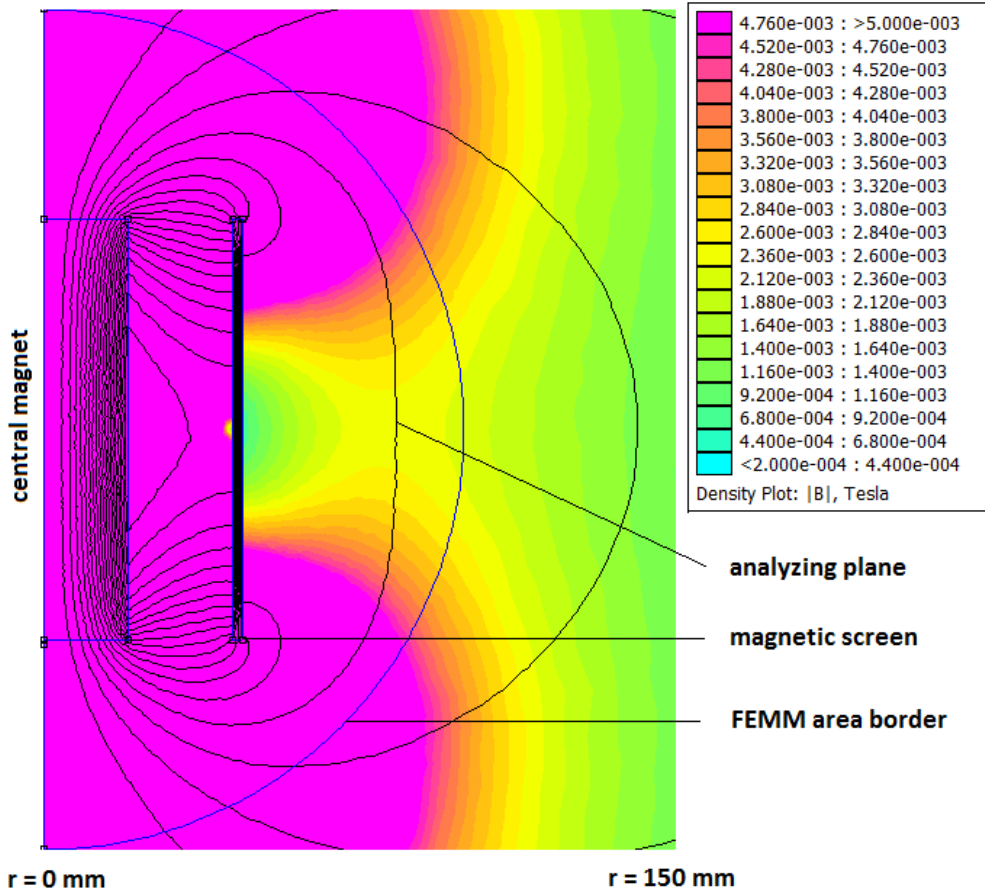


Figure 4: (150 × 200 mm) Cross section of the preliminary magnetic setup. The electrons are starting at the top end of the central magnet(left, $h = 100 \text{ mm}$, $r = 20 \text{ mm}$) and are guided to the detector located at its bottom end. The analyzing plane is shifted closer to the central magnet by the help of a magnetic screen($r_{inside} = 47.5 \text{ mm}$), with the same height as the central magnet. The geometry is divided into two semi circles, a smaller($r = 100 \text{ mm}$) and a bigger one($r = 300 \text{ mm}$), that define two areas of different grid size inside the FEMM program(see chapter 3).

The electrons start at a voltage of 18600V on the central magnet at ($r = 12.6 \text{ mm}$, $z = 50 \text{ mm}$) and are then retarded by the electric potential. To control the voltage in the analyzing plane, the outer wall and the magnetic screen are put on the same voltage ($V = 0$ for $|qU_0| = 18.6 \text{ keV}$).

As this experiments intended usage is the employment in student laboratories, this bachelor thesis intends to look for a more simple electrode setup. Also first simulations showed that electrons with high azimuthal angles did not pass the filter, because they would collide with the electrodes.

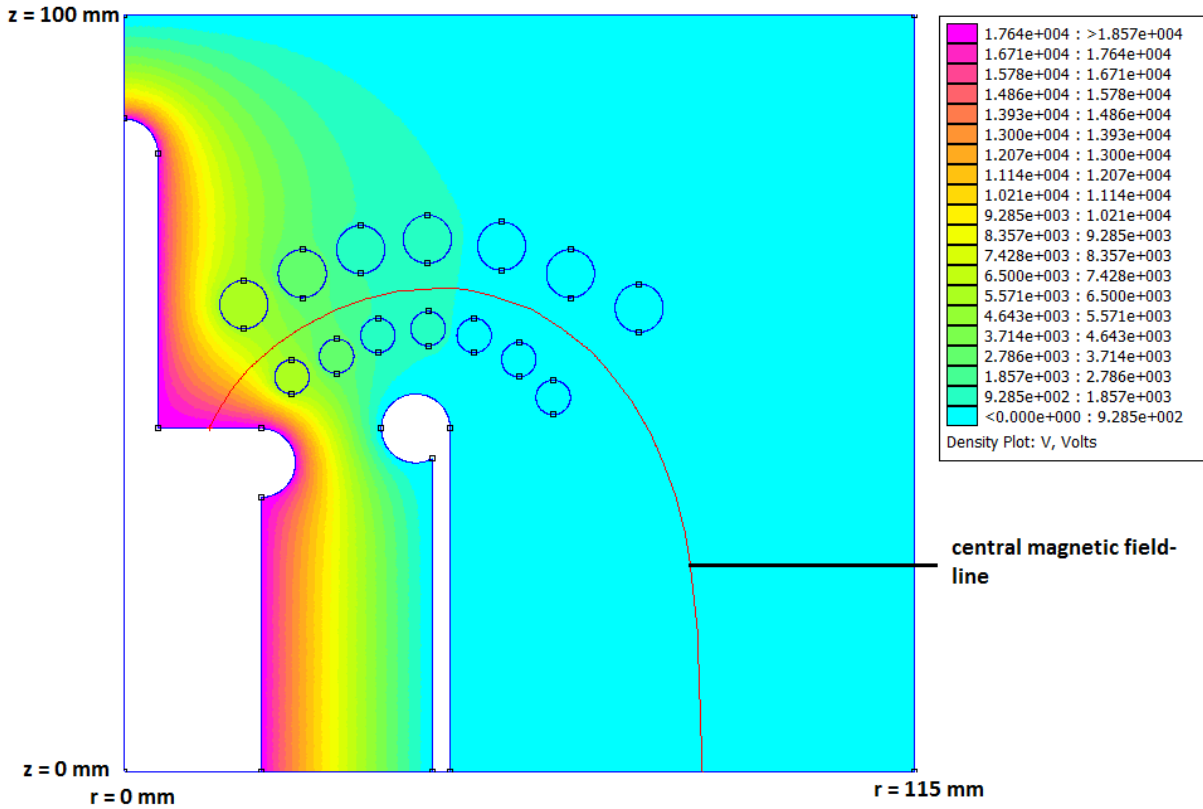


Figure 5: Preliminary electrostatic setup. The electrons start at the top of the central magnet (-18600 V) and are guided along the central fieldline to the analyzing plane. The toroid electrodes are placed around the central magnetic field line (red line). The outer walls of the vacuum chamber are set on ground level (0 V) to retard the electrons.

3. Electric potential and magnetic field calculations and particle tracking

3.1. FEMM

FEMM (finite elements method magnetics[Mee10]) allows the calculation of electric and magnetic fields in a finite geometry. It is also used as a solution for heat flow problems. The calculation is done by dividing the geometry into discrete sub regions ('elements') whose connection points are called 'nodes'.

To find the solution of the potential inside the whole geometry a set of linear elemental functions is set, as an ansatz for the wanted solution inside each element. These functions will then be solved in regard to the initial conditions that are set for the geometry.

3.1.1. Preprocessor

The preprocessor is used to define the geometry, boundary conditions and materials used inside the model (figure 6 shows a screen shot of the preprocessor). FEMM is not able to create 3-dimensional pictures, but can create models for 3-dimensions if the problem possesses cylindrical symmetry or is infinitely long with a constant cross section.

The geometry is defined by placing points that can be connected by straight or curved lines. Curved lines are defined by the arc angle that they close in between the two connecting points. For every line a boundary condition can be set (for a look at all boundary conditions look at the FEMM wiki²). The boundary condition that was used in the scope of this bachelor thesis is the ('mixed') boundary condition,

$$\left(\frac{1}{\mu_0\mu_r}\right)\frac{\partial A}{\partial r} + c_1A + c_0 = 0, \tag{16}$$

where μ_0 is the vacuum permeability, μ_r is the relative permeability of the material and c_0, c_1 are coefficients. FEMM can only calculate fields inside a finite area, but the magnetic problem that is faced creates a field that goes to 0 in an infinite distance. Luckily an analytical solution in a finite distance r for a field with this kind of boundary condition exists. In 2-dimensional polar coordinates (r, θ) it takes the form:

$$A(r, \theta) = \sum_{n=1}^{\infty} \frac{a_n}{r^n} \cos(nr + \alpha_n). \tag{17}$$

By differentiating this form in respect to r and only looking at the leading harmonic n we get

$$\frac{\partial A}{\partial r} + \frac{n}{r}A = 0. \tag{18}$$

²www.femm.info/wiki

Looking at equation 16 we see that this is the form given in the mixed boundary condition, which leads to the following coefficients:

$$c_0 = \frac{n}{\mu_0 r_0},$$

$$c_1 = 0,$$

where r_0 is the radius of the area that is modeled.

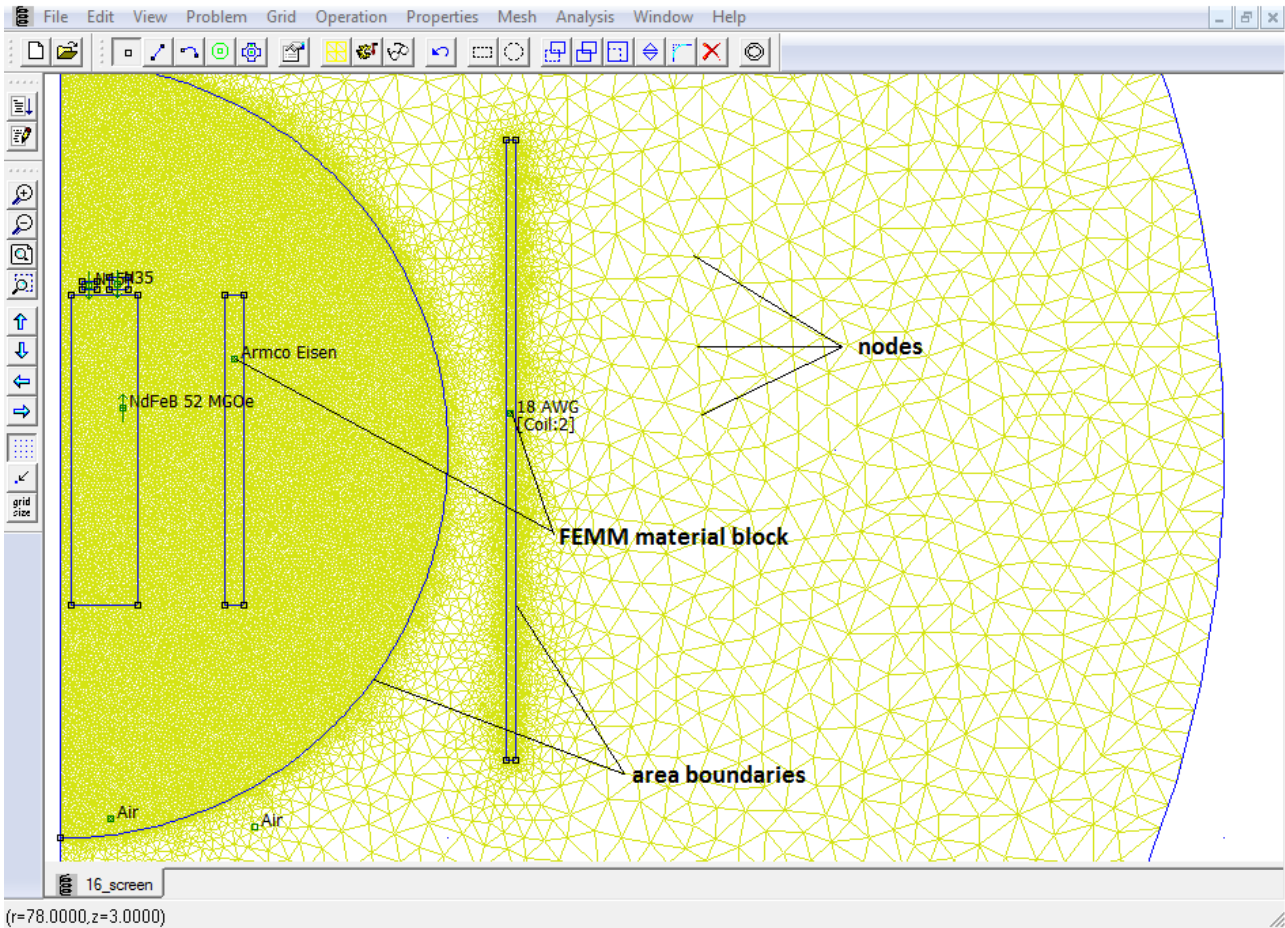


Figure 6: Screen shot of the preprocessor in the FEMM program, for a magnetic problem. The yellow grid shows the borders of the subregions in which the fields will be calculated. The green dots are elements in the program allowing the assignment of the material for the surrounding area. The blue lines define a region with its own material and grid size.

The field created in a model is of course dependent on the materials used. FEMM already offers a library of predefined materials, but also the option of adding new materials to the library.

The permanent magnetic materials in FEMM are categorized after their energy product $E = BH_{max}$, the maximum product of the magnetic flux density B and magnetic field strength H that can be simultaneously achieved as shown in figure 7.

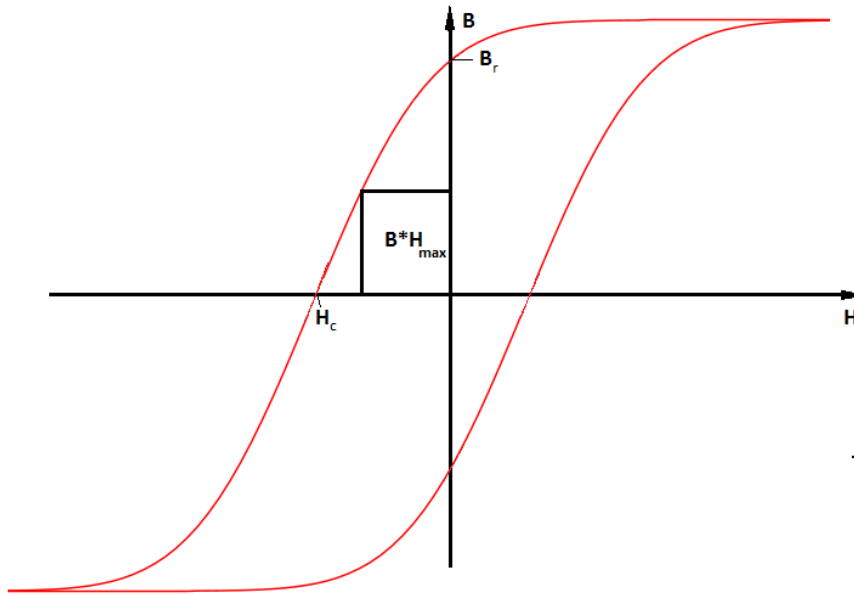


Figure 7: Maximal Energyproduct, $B \cdot H$ that can be simultaneously achieved, of a permanent Magnet visualized in its hysteresis curve.

The energy product is given in MGOe, where Oersted $1 \text{ Oe} = 1000/4\pi \text{ A/m}$ is an older unit giving the magnetic field strength and Gauss $1 \text{ G} = 10^{-4} \text{ T}$ is used as a unit for the magnetic flux density. The energyproduct has a unit J/m^3 , or energy per volume.

An area can also be assigned to a circuit in the magneto-static processor to, for example: model a coil. The circuit is either a serial or a parallel circuit and otherwise only defined by the strength of the current.

3.1.2. Postprocessor

Fields calculated by FEMM are then displayed in the postprocessor, where all the field values are stored. The readout of these values can be done in the postprocessor or by using the script-language Lua³. A Lua interpreter is embedded into the femm program. The Lua-commands also allow to write the field data at the requested points into a data or text file. This is used to access the field values inside the simulation program.

A lot more functions are available in FEMM, for a complete overview look at the femm manual.

³www.lua.org

3.2. Particle tracking

Inside an electromagnetic-field a particle with the charge q experiences the Lorentz-force

$$\vec{F} = m \begin{pmatrix} \ddot{x} \\ \ddot{y} \\ \ddot{z} \end{pmatrix} = q(\vec{v} \times \vec{B} + \vec{E}). \quad (19)$$

Taking a look at the force acting on a particle induced by the magnetic field, we can see that it is always perpendicular to the velocity vector. This leads to a circular motion around the magnetic field line. This motion is called cyclotron motion and its radius is described by

$$r_{cyc} = \frac{mv_{\perp}}{qB} = \frac{v_{\perp}}{\omega}, \quad (20)$$

where m is the mass of the electron, v_{\perp} the velocity component perpendicular to the magnetic field and ω is the frequency of the perpendicular motion.

Since equation (19) cannot be analytically solved, a numerical approximation is needed. Here the 4-th order Runge-Kutta-method was chosen. It approximates the solution of a first order ordinary differential equation (ODE) $\frac{d}{dx}y(x) = f(x, y)$ over an Interval from x_0 to $x_0 + h$ from a given solution at $y(x_0) = y_0$ and the knowledge of the derivative at all points.

Other methods solving this problem exist, but the Runge-Kutta-method was chosen, because it offers the best precision for the accuracy and time effort that is desired in the implementation as well as in the simulations. It is also a well-known method used, for example in the KASSIOPEIA tracking system used for the KATRIN-experiment.

The easiest way to approximate the solution for the problem mentioned above is the Euler formal

$$y(x_0 + h) = hf(x_0, y_0) + y(x_0). \quad (21)$$

However it only uses the derivative at the start point of the interval, which makes it an asymmetrical method not used in actual simulations. The error of the Euler formal is of order $\mathcal{O}(h^2)$. Methods with an error of $\mathcal{O}(h^{n+1})$ are of n -th order. To get to the 4-th order and gain more precision, the idea of the runge-kutta-method is to do 3 intermediate steps and use the derivative and the approximated solution at the points reached to get closer to the exact solution, as picture 8 shows. Mathematical this leads to the following equations:

$$k_1 = hf(x_0, y_0) \quad (22)$$

$$k_2 = hf\left(x_0 + \frac{h}{2}, y_0 + \frac{k_1}{2}\right) \quad (23)$$

$$k_3 = hf\left(x_0 + \frac{h}{2}, y_0 + \frac{k_2}{2}\right) \quad (24)$$

$$k_4 = hf(x_0 + h, y_0 + k_3) \quad (25)$$

$$y(x_0 + h) = y(x_0) + \frac{k_1}{6} + \frac{k_2}{3} + \frac{k_3}{3} + \frac{k_4}{6} + \mathcal{O}(h^5) \quad (26)$$

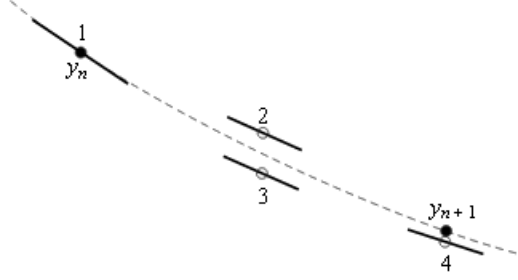


Figure 8: Figure of the trial steps taken in the 4th order Runge-Kutta method. y_n shows the starting position, while points 2, 3, and 4 show the trial steps taken, after the evaluation of the derivative in the points reached before. y_{n+1} is the final function value that is calculated. Figure taken from [PTVF92].

Now equation (19) is a second order ODE in three dimensions, but every ODE of n -th order, $y^{(n)} = F(x, y, y', \dots, y^{(n-1)})$, can be transformed into a first order ODE by the substitution $y_i = y^{(i-1)}$, where $y^{(n)}$ is the (n) th derivation of y . Now $y'_n = F(x, y, y_1, \dots, y_n)$ is a first order ODE. Applying this to (19) we get the functions

$$\vec{y} = \begin{pmatrix} y_1 \\ y_2 \\ y_3 \\ y_4 \\ y_5 \\ y_6 \end{pmatrix} = \begin{pmatrix} x \\ y \\ z \\ v_x \\ v_y \\ v_z \end{pmatrix} \quad (27)$$

and therefore

$$\vec{y}' = \begin{pmatrix} y_4 \\ y_5 \\ y_6 \\ \frac{q}{m}(y_4 B_z - y_5 B_y + E_x) \\ \frac{q}{m}(y_5 B_x - y_3 B_z + E_y) \\ \frac{q}{m}(y_3 B_y - y_4 B_x + E_z) \end{pmatrix}. \quad (28)$$

Now another factor deciding the precision of this numerical solution is the choice of the step size h . Of course if h is too big, the precision will diminish, and if h becomes too small, unnecessary much time will be spent on the calculation. To set h into a physical context we see that it defines a time interval over which the ODE will be integrated. If we look at the cyclotron frequency (equation 20), because the cyclotron motion is dominant while the electron drifts along the field line, we pick

$$h = \frac{1}{\omega n}, \quad \text{with } n \text{ being any even, positive number.} \quad (29)$$

This way we approximate the circular motion with a n -edged polygon.

4. Design of a tabletop MAC-E-filter

4.1. Magnetic setup

The magnetic setup for the MAC-E-filter can be seen in picture 9 and possesses the same symmetry as already shown in section 2.2. The mentioned field values refer to the values occurring along the central field line. All magnets that are shown here are neodymium-iron-boron (NdFeB) magnets and can be found in the assortment of HKCM Engineering company ⁴.

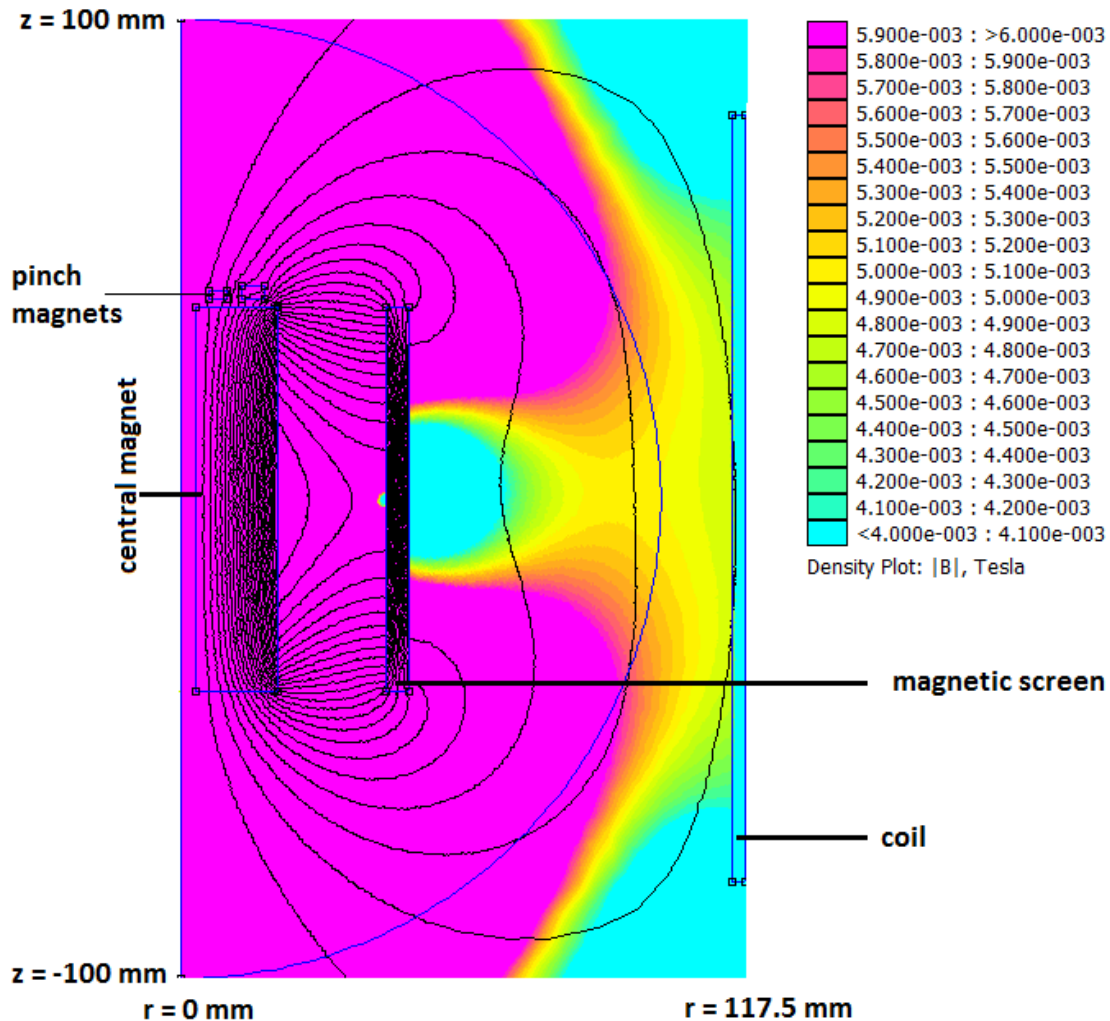


Figure 9: Simulated magnetic setup. On the top end of the magnet the electrons are started and pass through the pinch magnets. The field in the analyzing plane is supported by a coil and shifted towards the central symmetry axis ($r = 0$ mm) by a magnetic screen.

⁴www.hkcm.de

The central magnet in this setup is a ring magnet, which possesses an energy product of 52 MGOe (this is the highest possible energy product for a NdFeB-magnet), a height of 80 mm, an inner radius of 3 mm and an outer radius of 20 mm. Above the north pole of the central magnet, two ring magnets form a pinch producing the highest field strength in the setup with $B_{max} = 0.915$ T. Both magnets are placed with 1.5 mm distance to the main magnet at $z = 41.5$ mm. The inner ring magnet has an energy product of 45 MGOe, an inner radius of $r_i = 5.65$ mm and an outer radius of $r_o = 9.4$ mm, its height is $h = 2$ mm. Likewise the geometry of the outer ring magnet is $r_i = 12.5$ mm, $r_o = 17.5$ mm and $h = 3$ mm, but its energy product is 35 MGOe. Figure 10 shows a close-up picture of the two ring magnets. Even though the outer magnet possesses a lower energy product, the produced field elevation is nearly equally distanced between the two ring magnets, since the lower energy product is compensated by the bigger volume of the outer ring.

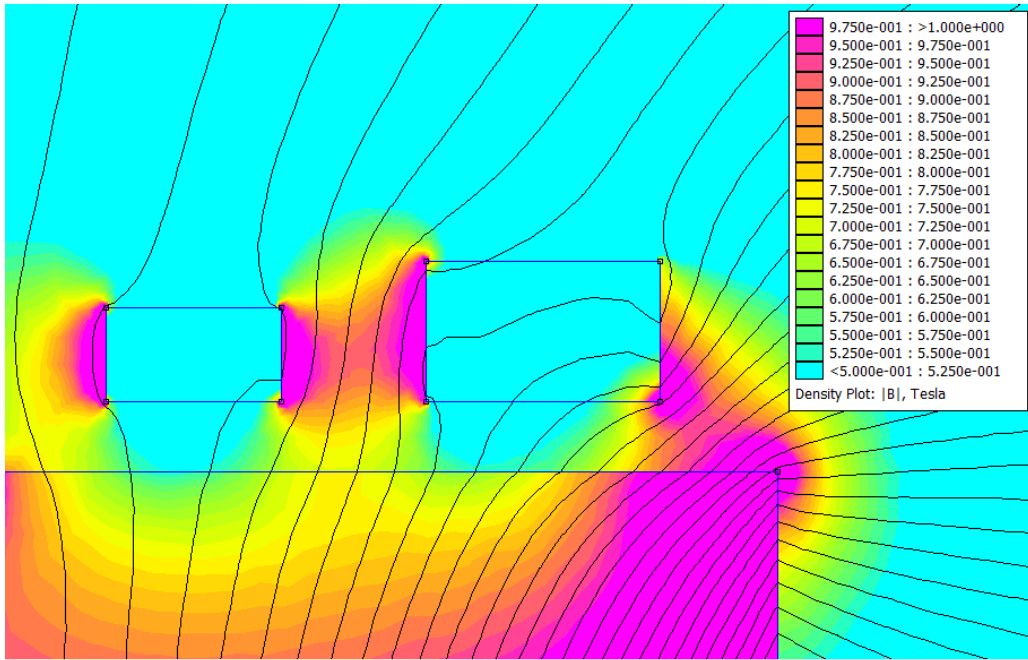


Figure 10: (14 × 22 mm)screen shot of the top end of the central magnet. Here the electrons are started and then pass through the pinch, generated by the two pinch magnet rings. On the left the inner magnet ring can be seen and on the right the outer ring is visible.

The central field line exits the main magnet at (10.19, 40) mm at a source field strength of 0.75 T and then travels through the pinch magnet, with a field strength of 0.915 T. Using equation(14) all electrons with angles over $\Theta_{max} = 64.86^\circ$ will be reflected by the pinch. Upon reaching the analyzing plane(96.7, 0) mm, the field strength drops to about 5 mT. The theoretical energy resolution (equation 8) of this setup is then

$$\Delta E = 18600 \text{ eV} \cdot \frac{0.005 \text{ T}}{0.914 \text{ T}} \approx 102 \text{ eV}. \quad (30)$$

As can be seen in figure 9, the field in the analyzing plane is supported by an air-coil placed

on the outside wall of the vacuum chamber(18 AWG⁵ copper wire, 2 turns and -250 A). The magnetic screen has an inner radius of 42.5 mm, is 5 mm thick and is composed of Armco iron. A resizing of the screen could bend the field lines strong enough to fit inside the spectrometer, but it would reduce the field strength even further, which would lead to a bigger cyclotron radius. The implications of this are discussed in chapter 4.3.

4.2. Electrostatic setup

The electric setup can be seen in figure 11. Contrary to the preliminary setup, the central magnet and the pinch magnet rings are set to ground level (0 V), because the readout of the detector will be simplified this way. The pinch magnet also needs to remain on ground level, because electric retardation inside the pinch magnet would alter the pinch angle, which would violate the condition for calculating the reflection angle inside the pinch and also strongly violate the adiabaticity of the filter. Still a difference in voltage of ≈ 700 V remains along the field line. The consequences of this are shown and discussed in the next chapter.

The electrodes in this setup are copper wires imprinted on printed circuit boards (pcb) of FR4-material (relative permittivity $\epsilon_r = 4.7 \frac{\text{As}}{\text{Vm}}$), which is a epoxy impregnated glass-fiber matte.

Overall, there are 12 electrodes on the lower pcb and 27 on the upper one. The exact voltage of each electrode can be seen in the tables 3 and 2 respectively. The voltage change on both pcbs is $\Delta V = (-12970 \text{ V}) - (-18310 \text{ V}) = 5340 \text{ V}$. Even though the electrodes are not symmetrically aligned alongside the central field line as in the preliminary setup, the produced field is estimated to mostly parallel to the magnetic field, so that the adiabatic retardation is still ensured.

The magnetic screen and the outer wall of the spectrometer are also set on electric potential to set the voltage in the analyzing plane. For an analyzing voltage $qU_0 = 18600 \text{ eV}$ the wall and the screen are both set on -18635.5 V .

⁵American Wire Gauge

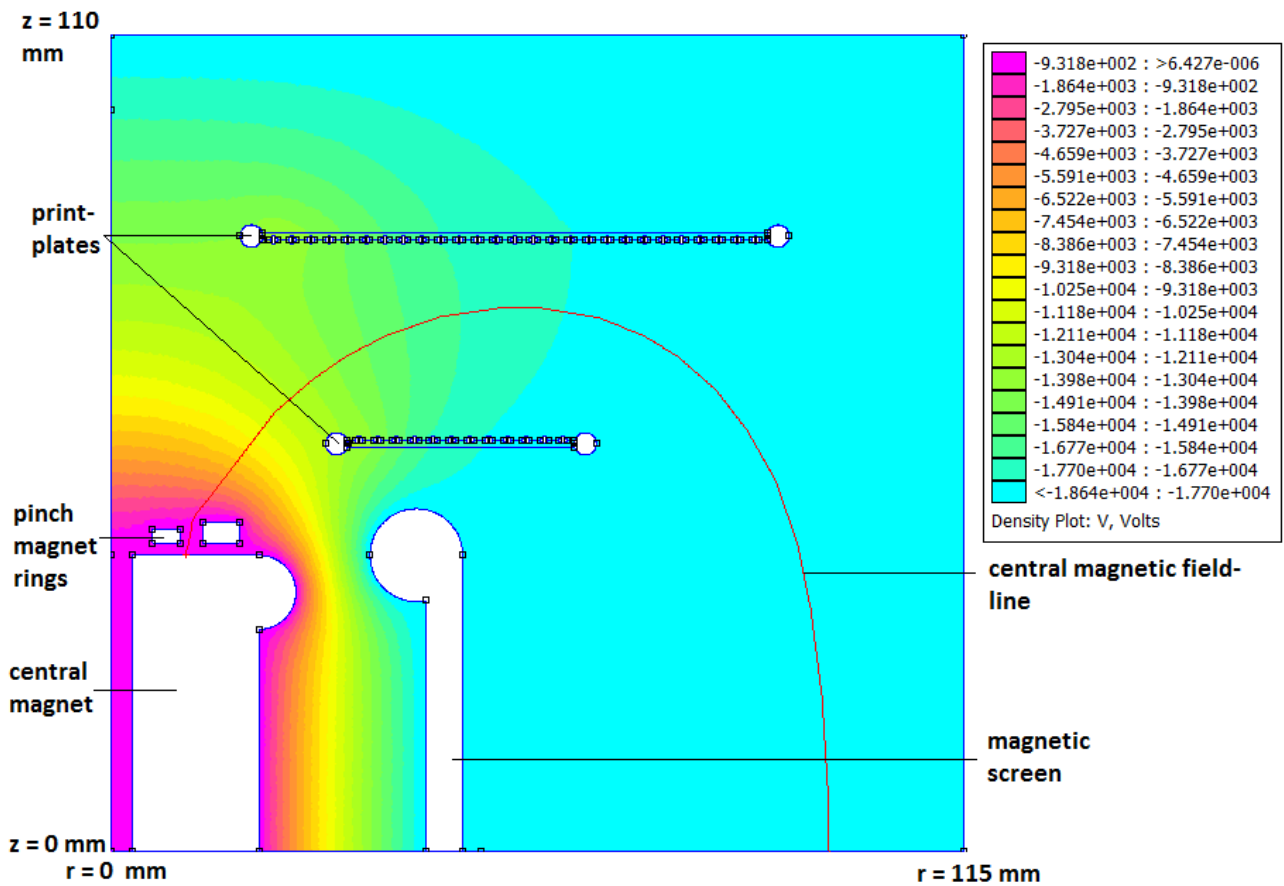


Figure 11: Simulated electrostatic setup. On the top of the central magnet the electron start on ground level (0 V) and then pass through the pinch magnets, that are also set on ground level. The retarding electrodes are mounted on printplates. The outer Wall ($r = 115$ mm) and the magnetic screen ($r = 45$ mm) are set on negative potential to generate the analyzing Voltage qU_0 .

4.3. Particle tracks

The program which is used to simulate the electron tracks, is written in the C++-language. The whole code can be seen in the appendix.

To analyze the transmission function of the MAC-E-filter, simulation were run for different surplus energies of the electron. The analyzing voltage was set to $qU_0 = 18600$ eV, the energy of the electrons ranged from 18600 eV to 18745 eV , with a step size of 5 eV. For every surplus energy the starting angle was varied from 0° to 90° in 5° steps. The result is pictured in figure 12.

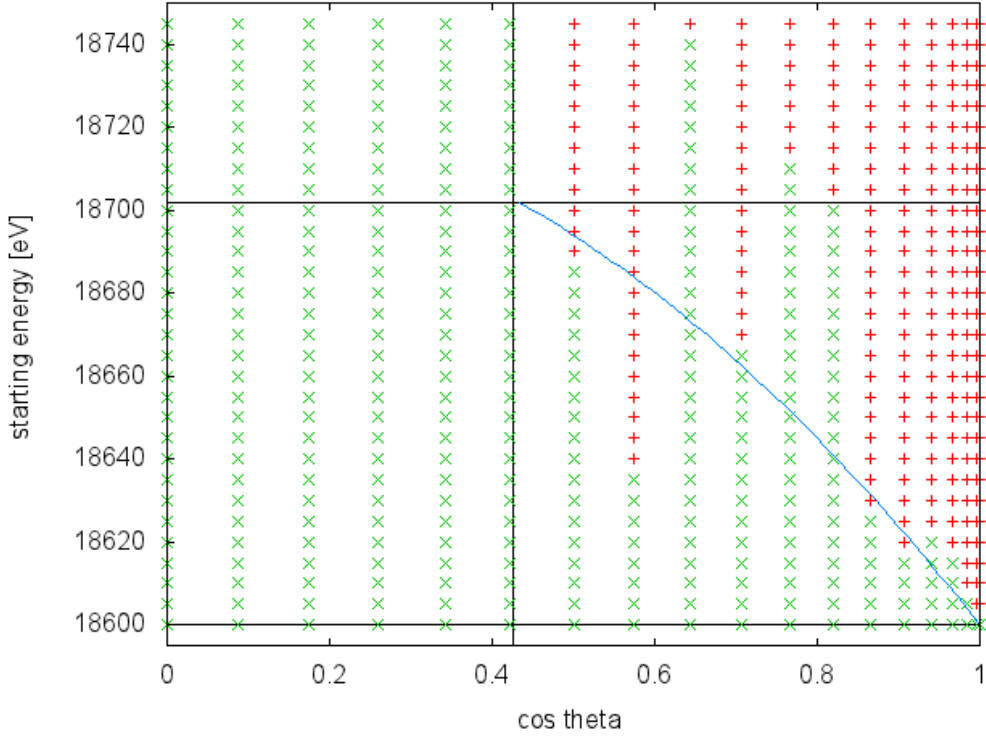


Figure 12: Simulated transmission of electrons through the MAC-E-filter setup. A red cross marks an electron, with the corresponding starting energy and starting angle θ_s , that passes through the filter. A green cross marks the electrons that do not pass. The blue line represents the theoretically expected border(derived from equation (15)), where all electrons above the line should pass the filter and the ones below should not.

Now the tracks with starting angles 35° , 40° , 50° and 55° differ strongly from the expected behavior. While electrons with a starting angle of 50° , 40° and 35° are starting to pass the filter at a much higher surplus energy than expected, electrons with a starting angle of 55° show a different behavior and pass the filter with lower surplus energies than expected.

By taking a look at the relative change of the magnetic momentum

$$\Delta\mu = \frac{\mu - \mu_0}{\mu_0}, \quad (31)$$

we can take a closer look at the energy transformation along the track of the electron. By

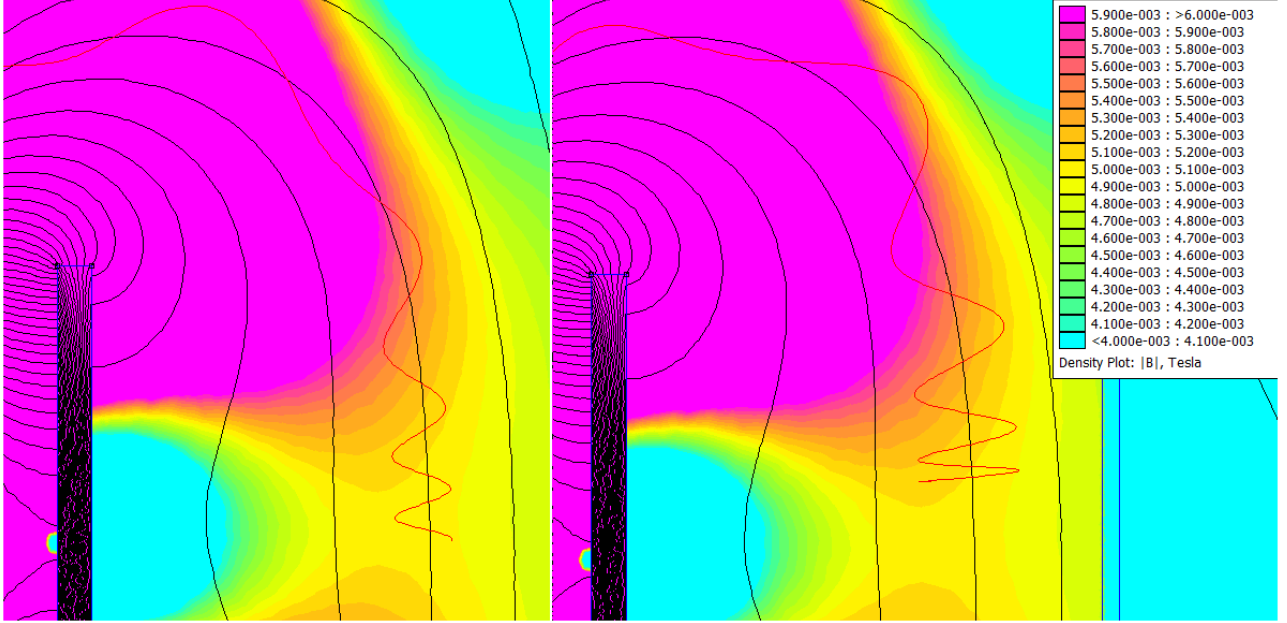


Figure 13: Simulated track (red line) for $\theta = 55^\circ$, $E_{start} = 18640$ eV (left) and $\theta = 40^\circ$, $E_{start} = 18710$ eV (right) approaching the analyzing plane

looking at equation 6 we can derive that the perpendicular energy of an electron with a changed magnetic moment $\Delta\mu$ is

$$E_{\perp} = E_{\perp,ad}(\Delta\mu + 1)\frac{B_{max}}{B_{src}}, \quad (32)$$

expressed in terms of the perpendicular energy in the totally adiabatic case $E_{\perp,ad}$. This helps estimating the violation of the adiabatic criteria and the transformation of the energy. By looking at $\Delta\mu$ along the whole track (figure 14) we can see that the magnetic moment is oscillating along the field, which is expected due to the cyclotron motion of the electron, but at two points this oscillation is interrupted.

The first one is at the very beginning of the track, when the electron passes through the pinch magnet. Here the electron experiences a strong shift in the magnetic field strength and the magnetic field is very inhomogeneous over one cyclotron motion. Especially when the electron leaves the pinch, an abrupt change of the magnetic moment can be seen. A look at the electron track at this point (figure15) shows that the electrons pass through a change of about 0.2 T inside one cyclotron motion, while exiting the pinch. Afterwards the magnetic moment no longer oscillates around its initial value μ_0 , but around the value it takes on after exiting the inhomogeneous field area of the pinch. This can lead to either a lower magnetic moment ($\theta = 55^\circ$, $E_{start} = 18640$ eV) or an increase ($\theta = 40^\circ$, $E_{start} = 18710$ eV), as can be seen in the simulation.

At the second point the electron, due to its cyclotron motion, enters into a very inhomogeneous field and reaches a local minimal field value of nearly the analyzing field strength and then moves back into a higher B-field. This happens repeatedly as can be seen in picture 13.

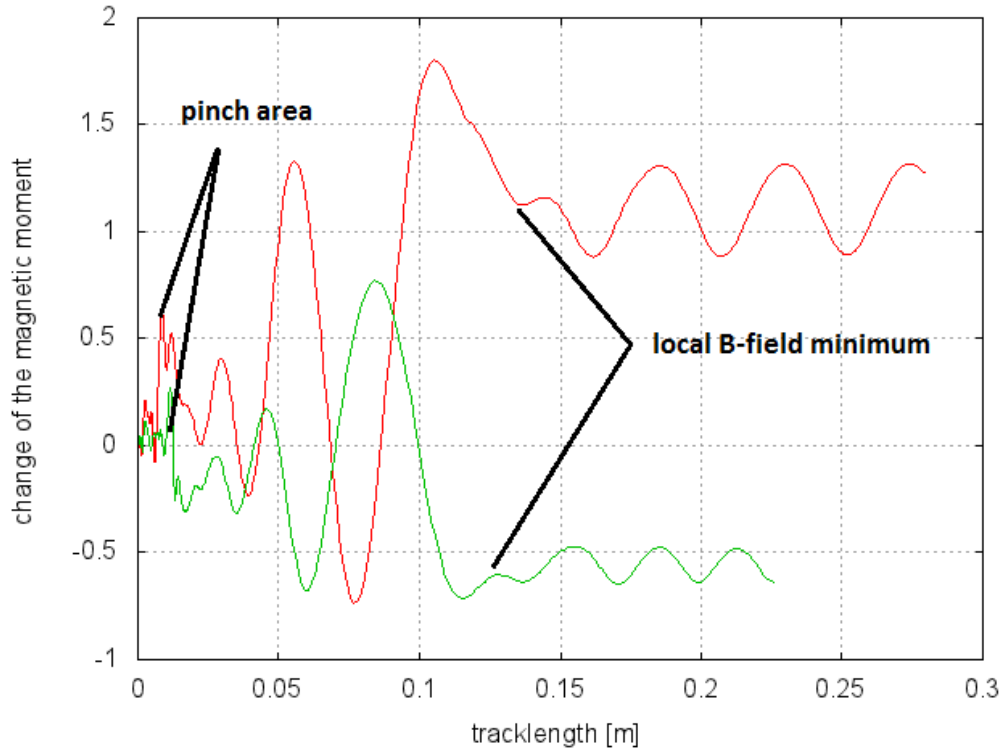


Figure 14: relative change of the magnetic moment along the track for $\theta = 40^\circ$ and a starting energy of 18710 eV (red line) and $\theta = 55^\circ$ and a starting energy of 18640 eV (green line)

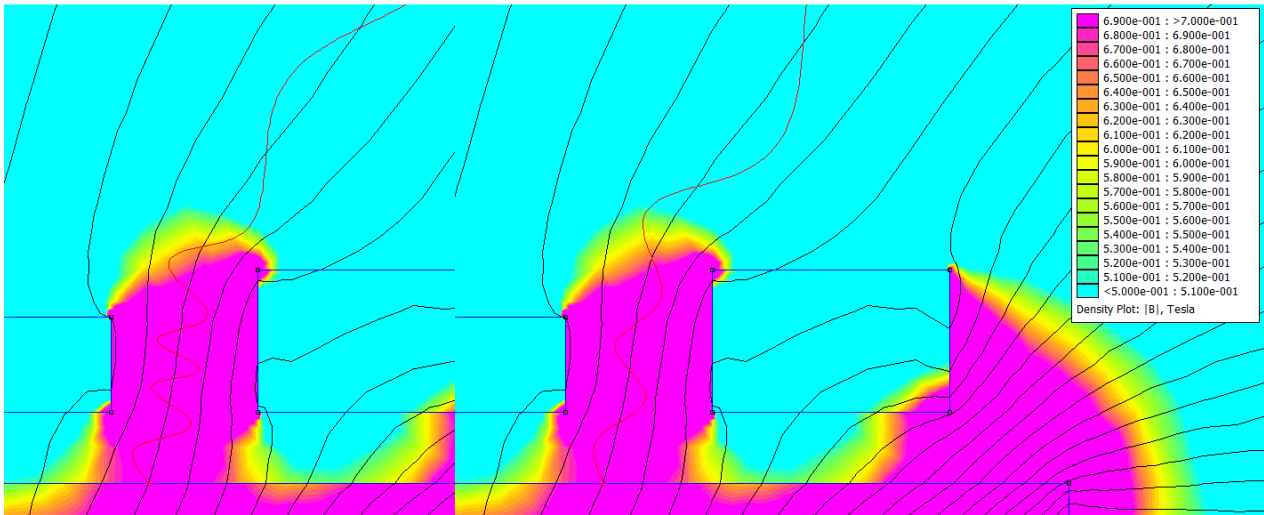


Figure 15: Simulated track (red line) for $\theta = 40^\circ, E_{start} = 18710$ eV and $\theta = 55^\circ, E_{start} = 18640$ eV at the start point, passing through the pinch magnet.

As discussed before, this violates the MAC-E-filter principle since the electron should only experience a decreasing field until it reaches the analyzing plane. Also when the electron travels from a lower to a higher field strength, parallel energy is reconverted into perpendicular energy. This means the perpendicular energy of the electron oscillates between two points, depending on the magnetic field strengths it oscillates between, which can also be seen in the oscillation of the magnetic moment.

The discussed effects can decrease or increase the transmission of an electron through the analyzing plane. If the oscillation of the magnetic moment is at a minimum, when the electron reaches the minimum of the B-field (as seen in picture 15, green line), the perpendicular energy will then oscillate at a lower offset, as if the magnetic moment is at a maximum (picture 15, red line). So these effects are not dependent on the starting energy or starting angle the electron has, but rather on the path of flight it takes through the filter, which is not predictable from the initial conditions.

5. Conclusion and outlook

The analysis showed that the tested setup does not allow for an adiabatic transmission for all electrons, which would lead to a deformed spectrum. Also the impact on the transmission of the responsible effects cannot be foreseen by looking at the initial conditions, which disqualifies this setup for actual use.

Seeing that the cyclotron motion causes the non-adiabatic transformation of energy, a smaller cyclotron radius in the vicinity of the analyzing plane would be needed to improve the performance of this setup. This could be achieved by decreasing the energy even stronger until the electron reaches the inhomogeneous B-field, but even if this could be achieved the electrons on the neighboring field lines would still experience strongly inhomogeneous fields and thus deform the measured spectrum.

Another possibility would be to increase the analyzing field strength, which would reduce the energy resolution, but improve the homogeneity of the field in the analyzing plane.

The pinch magnet is another part of the setup that causes a non-adiabatic motion. A smoother decrease of the field strength is needed, by either decreasing the overall pinch strength, which in return would result in a bigger cutoff angle and also decrease the energy resolution, or to abstain from using a pinch. In the small geometry of this setup the difference in track length may not be significant and thus it could in principle work without a pinch. The conducted simulations did not consider background implications and the pinch magnet was included on the experience from the foregone MAC-E-filter experiments, so this would have to be discussed in another thesis.

The electrode system in the setup was simplified in regards to the first setup, but a more complex setup could lead to an electric field aligned more parallel to the magnetic field. Since the problems in the magnetic setup are clearly dominant, the differences are not directly visible and so the electrostatic setup needs further investigation.

Overall the field strengths reached in this setup seem too strong to allow an adiabatic transmission of electrons. Settling with a lower resolution would give another chance to this setup. An alternative setup to the discussed one, is shown in figure 16. Two identical magnets are placed inside a vacuum chamber, with the same orientation. With a distance of $r = 100$ mm, an electrode is placed in the space between the magnets. Thus creating the analyzing plane of this setup in the middle of the space between the magnets, where the magnetic field strengths drops to a minimum.

This setup is very similar to the KATRIN setup, but another electrode at the height of the analyzing plane is added, to support the electric field. Thus the analyzing plane is a circular ring between the two electrodes.

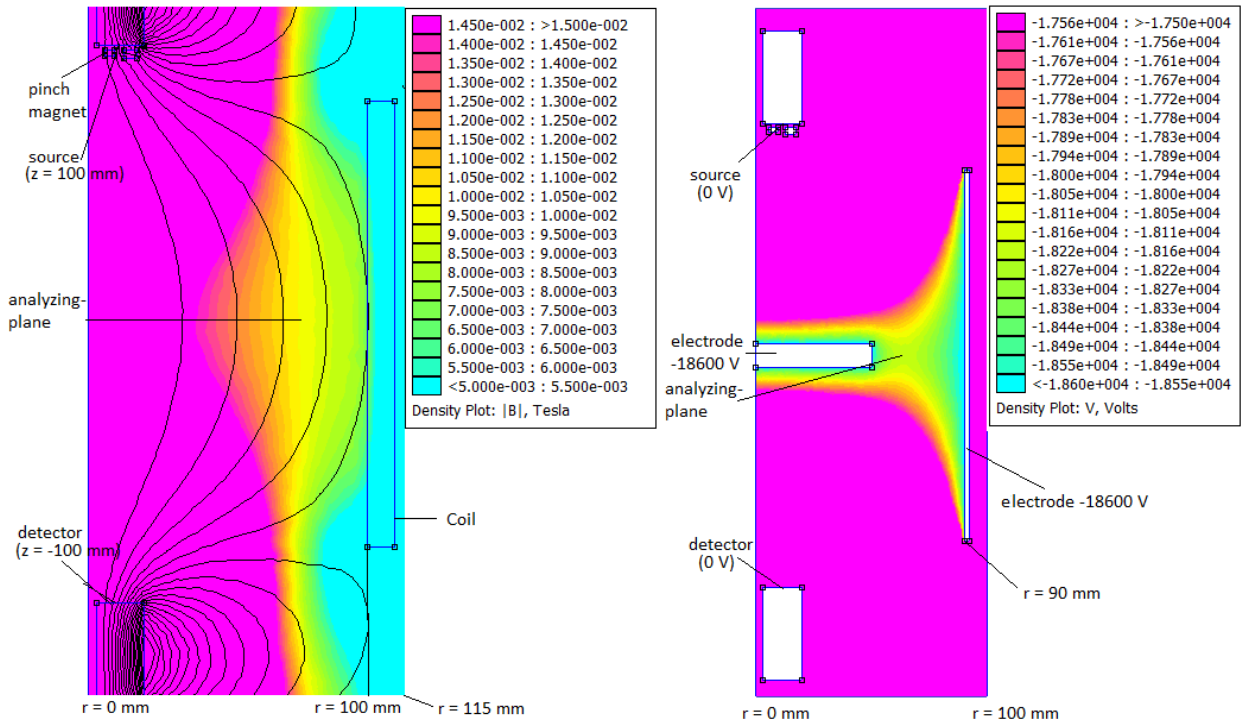


Figure 16: MAC-E-filter design, magnetic setup(left) from the symmetry axis($r = 0$ mm) to $r = 115$ mm and the electrostatic setup(right) from the symmetry axis to $r = 100$ mm. The electron start from the bottom of the upper magnet($z = 100$ mm) and are guided to the top of the lower magnet($z = -100$ mm). Two electrodes on -18600 V retard the electrodes in the analyzing plane ($z = 0$ mm).

A. Electrode voltages

Electrode	Voltage [V]	Electrode	Voltage [V]
1	-12970	15	-17520
2	-13478	16	-17605
3	-13986	17	-17690
4	-14494	18	-17775
5	-15002	19	-17855
6	-15510	20	-17936
7	-15842	21	-18015
8	-16173	22	-18090
9	-16505	23	-18165
10	-16800	24	-18200
11	-16940	25	-18233
12	-17090	26	-18267
13	-17230	27	-18310
14	-17375		

Table 2: retardation voltages of the electrodes on the upper printed circuit board in the setup

Electrode	Voltage [V]
1	-12970
2	-14190
3	-15412
4	-16300
5	-16905
6	-17245
7	-17562
8	-17760
9	-17955
10	-18145
11	-18235
12	-18310

Table 3: retardation voltages of the electrodes on the lower printed circuit board in the setup

References

- [Cha14] J. Chadwick. Distribution in intensity in the magnetic spectrum of the beta-rays of radium. *Verh.Dtsch.Phys.Ges.(Germany)*, 16:383, 1914.
- [D⁺13] G. Drexlin et al. Current Direct Neutrino Mass Experiments. *Advances in High Energy Physics 2013,293986*, 2013.
- [EW27] C.D. Ellis and W.A. Wooster. The Average Energy of Disintegration of Radium E. *Proc.R.Soc.*, 16:109, 1927.
- [Fer34] E. Fermi. Versuch einer Theorie der Beta-Strahlen. *Z.Phys.*, 88:161, 1934.
- [K⁺05] Ch. Kraus et al. Final results from phase II of the neutrino mass search in tritium beta decay. *Eur.Phys.J.C*, 40,447468, 2005.
- [KAT04] KATRIN Collaboration. KATRIN Design Report. 2004.
- [Lob03] V.M. Lobashev. The search for the neutrino mass by direct method in the tritium beta-decay and perspectives of study it in the project KATRIN. *Nucl.Phys.A*, 719:C153–C160, 2003.
- [Mee10] D.C. Meeker. Finite Element Method Magnetics. *Version 4.2*, 2010.
- [P⁺92] A. Picard et al. A solenoid retarding spectrometer with high resolution and transmission for keV electrons. *Nuclear Instruments and Methods in Physics Research*, pages 345–358, 1992.
- [Pau64] W. Pauli. Wolfgang Pauli, Collected Scientific Papers. *Vol. 2, Interscience, New York*, 16:1316, 1964.
- [PTVF92] W.H. Press, S.A. Teukolsky, W.T. Vetterling, and B.P. Flannery. *NUMERICAL RECIPES IN C++: The Art of Scientific Computing, Second Edition*. Cambridge University Press, 1992.
- [RC59] R. Reines and C.L. Cowan. Free Antineutrino Absorption Cross Section. First Measurement of the Free Antineutrino Absorption Cross Section by Protons. *Phys.Rev.*, 113:273, 1959.

Listing 1: rk4.cpp

```

1 #include "stdafx.h"
2 #include <fstream>
3 #include <iostream>
4 #define _USE_MATH_DEFINES
5 #include <math.h>
6 #include <vector>
7 #include <sstream>
8
9 using namespace std;
10
11 // approximates the field values at (r,z) 'field' from the stored field values
12 // ↪ 'Field'
13 // through bilinear interpolation
14 void field_approx(double r, double z, double &field, vector<double>& Field){
15     double app1, app2, rc, zc;
16     //locate next point of the field value grid next to the current electron
17     // ↪ position
18     rc = (r*1e4 - fmod(r*1e4, 1))*1e-4;
19     zc = (z*1e4 - fmod(z*1e4, 1))*1e-4;
20     //get array key of the field value of the next grid point
21     int R = rc*1e4;
22     int Z = zc*1e4;
23     int K0 = R+1152*Z;
24     //bilinear interpolation
25     try{
26         app1 = Field.at(K0) + ((r-rc)*(Field.at(K0+1) - Field.at(K0)))/0.0001;
27         app2 =
28             ↪ Field.at(K0+1152) + (r-rc)*(Field.at(K0+1153) - Field.at(K0+1152))/0.0001;
29     }catch(out_of_range e){
30         throw e;
31     }
32     field = app1 + (z-zc)*(app2-app1)/0.0001;
33 }
34
35 //readout of several variables
36 void param(vector<double> y, vector<double>& BR, vector<double>& BZ,
37     ↪ vector<double> V,
38     double& v_par, double& v_nor, double& B, double& Volt, double& br, double&
39     ↪ bz,
40     double& er, double& ez, vector<double>& ER, vector<double>& EZ){
41     double r = pow(y[0]*y[0] + y[1]*y[1], 0.5);
42     double z = y[2];
43     try{
44         field_approx(r, z, br, BR);
45         field_approx(r, z, bz, BZ);
46         field_approx(r, z, er, ER);
47         field_approx(r, z, ez, EZ);
48         field_approx(r, z, Volt, V);
49     }catch(out_of_range e){
50         throw e;
51     }
52
53     // b-field value
54     B = pow(br*br + bz*bz, 0.5);
55
56     //calculate parallel v_par and perpendicular v_nor velocity components
57     //through the scalar product with the b-field values

```

```

53     double v_tot = pow(y[3]*y[3]+y[4]*y[4]+y[5]*y[5],0.5);
54     v_par = ((y[3]*br*y[0]/r+y[4]*br*y[1]/r+y[5]*bz)/B);
55     v_nor = pow(v_tot*v_tot-v_par*v_par,0.5);
56 }
57
58 //calculates stepsize for the runge-kutta-method at a point y
59 // n is the number of steps that are taken to approximate one cyclotron motion
60 double stepsize(int n, vector<double> y,vector<double>& BR, vector<double>& BZ){
61     const double q = 1.602176e-19;//absolute of the electron charge [A*s = C]
62     const double m = 9.109382e-31;//electron mass [kg]
63     double stepsize,B,br,bz;
64
65     //calculate position in (r,z)-grid
66     double r = pow(y[0]*y[0]+y[1]*y[1],0.5);
67     double z = y[2];
68     //get field values at (r,z)
69     try{
70         field_approx(r,z,br,BR);
71         field_approx(r,z,bz,BZ);
72     }catch(out_of_range e){
73         throw e;
74     }
75
76     B = pow(br*br+bz*bz,0.5);
77     stepsize = m/(q*B*n);
78     return stepsize;
79 }
80
81 // get the derivative dydx of y
82 void derivs(vector<double> y, vector<double> &dydx, vector<double>& ER,
83     ↪ vector<double>& EZ
84     ,vector<double>& BR, vector<double>& BZ)
85 {
86     // go into (r,z) coordinate system
87     double r = pow(y[0]*y[0]+y[1]*y[1],0.5);
88     double z = y[2];
89     double er,Ez,br,Bz;
90
91     // approximate field data at y
92     try{
93         field_approx(r,z,er,ER);
94         field_approx(r,z,Ez,EZ);
95         field_approx(r,z,br,BR);
96         field_approx(r,z,Bz,BZ);
97     }catch(out_of_range e){
98         throw e;
99     }
100
101     // go back into (x,y,z) coordinate system
102     double Ex,Ey,Bx,By;
103
104     Ex = er*y[0]/r;
105     Ey = er*y[1]/r;
106     Bx = br*y[0]/r;
107     By = br*y[1]/r;
108
109     // calculate derivative components
110     const double q = -1.602176e-19;//A*s = C
111     const double m = 9.109382e-31;//kg

```

```

111     dydx[0] = y[3];
112     dydx[1] = y[4];
113     dydx[2] = y[5];
114     dydx[3] = (q/m)*(Ex+y[4]*Bz-y[5]*By);
115     dydx[4] = (q/m)*(Ey+y[5]*Bx-y[3]*Bz);
116     dydx[5] = (q/m)*(Ez+y[3]*By-y[4]*Bx);
117 }
118
119 // calculates angle between z-axis and b-field at (r,z)
120 double startAngle(vector<double>& BR, vector<double>& BZ, double r, double z){
121     const double pi = M_PI;
122     double br,bz;
123     field_approx(r,z,br,BR);
124     field_approx(r,z,bz,BZ);
125     // scalar product between (r,z)-vector and b-field vector
126     double alpha = acos(bz/pow(bz*bz+br*br,0.5))*180/pi;
127     return alpha;
128 }
129
130 //calculate start velocity for starting energy Ener,
131 //starting angle between momentum and b-field theta,
132 //starting azimuthal angle phi
133 void startvelocity(double Ener, double theta, double phi, double alpha,
    ↪ vector<double> &v){
134     const double pi = M_PI;
135     const double c = 299792458;// speed of light [m/s]
136     const double m = 510.998;// mass of the electron [keV/c^2]
137     double v0;
138     //calculate v using transformation from spherical coordinates to cartesian
    ↪ coordinates
139     //the velocity vector is calculated for a cartesian coordinate system with
    ↪ the b-field vector as the z-axis
140     double total_v = c*sqrt(2*Ener/m);
141     v[0] = total_v * sin((theta)*pi/180)*cos(phi*pi/180);// m/s
142     v[1] = total_v * sin((theta)*pi/180)*sin(phi*pi/180);
143     v[2] = total_v * cos((theta)*pi/180);
144     //transform the velocity components into the laboratory system
145     v0 = v[0];
146     v[0] = cos(alpha*pi/180)*v[0]+sin(alpha*pi/180)*v[2];
147     v[2] = cos(alpha*pi/180)*v[2]-sin(alpha*pi/180)*v0;
148 }
149
150 // calculation if the runge-kutta-method with the derivative dydx and the
    ↪ intial position y,
151 // the fieldvalues ER,EZ,BR,BZ and the stepsize h
152 void rk4(vector<double> &y, vector<double> &dydx, double h,
153     vector<double> &yout,vector<double>& ER,vector<double>& EZ,vector<double>&
    ↪ BR,vector<double>& BZ)
154 {
155     int i;
156     double xh,hh,h6;
157
158     int n=y.size();
159     vector<double> dym(n),dyt(n),yt(n);
160     hh=h*0.5;
161     h6=h/6.0;
162     xh=hh;
163     //first trial step with stepsize hh

```

```

164     for (i=0;i<n;i++) yt[i]=y[i]+hh*dydx[i];
165     try{
166         derivs(yt,dyt,ER,EZ,BR,BZ);
167     }catch(out_of_range e){
168         throw e;
169     }
170     //second trial step with stepsize hh
171     for (i=0;i<n;i++) yt[i]=y[i]+hh*dym[i];
172     try{
173         derivs(yt,dym,ER,EZ,BR,BZ);
174     }catch(out_of_range e){
175         throw e;
176     }
177     // third trial step with stepsize h
178     for (i=0;i<n;i++) {
179         yt[i]=y[i]+h*dym[i];
180         dym[i] += dyt[i];
181     }
182     try{
183         derivs(yt,dyt,ER,EZ,BR,BZ);
184     }catch(out_of_range e){
185         throw e;
186     }
187     // calculate final step
188     for (i=0;i<n;i++)
189         yout[i]=y[i]+h6*(dydx[i]+dym[i]+2.0*dym[i]);
190 }
191
192
193 int _tmain()
194 {
195     double r,z,erbuff,ezbuff,brbuff,bzbuff,vbuff;
196     vector<double> v(3);
197     char c;
198     const int pointnumber = 981504;//number of field data points
199     vector<double> ER(pointnumber);//radial electrical field vlaues
200     vector<double> EZ(pointnumber);//axial electrical field values
201     vector<double> BR(pointnumber);//raidal magnetic field values
202     vector<double> BZ(pointnumber);//axial magnetic field values
203     vector<double> V(pointnumber);//voltage values
204
205     //field data readout
206     int R = 0;
207     ifstream file_one ("Efin.dat", std::ifstream::in);//electric field data
208     while(file_one.good()){
209         file_one>>r>>z>>erbuff>>ezbuff>>vbuff;
210         ER[R] = erbuff;
211         EZ[R] = ezbuff;
212         V[R] = vbuff;
213         R++;
214         if(R == pointnumber)break;
215         file_one.get(c);
216     }
217     file_one.close();
218     R = 0;
219     ifstream file_two ("Bfin.dat", std::ifstream::in);//magnetic field data
220     while(file_two.good()){
221         file_two>>r>>z>>brbuff>>bzbuff;

```

```

222     BR[R] = brbuff;
223     BZ[R] = bzbuff;
224     R++;
225     if(R == pointnumber)break;
226     file_two.get(c);
227 }
228 file_two.close();
229
230 double h;//stepsize variable
231
232 double En[] = {18.6};//starting energy in keV
233 double theta[] = {40};//starting pinch angle in degrees
234 double phi[] = {0};//starting azimuthal angle in degrees
235
236 double rStart = 0.0102;//radial starting point
237 double zStart = 0.040;//axial starting point
238 double alpha = startAngle(BR,BZ,rStart,zStart);//starting angle between
    ↪ z-axis and B-field
239 double pinchangle;
240
241 for(int k = 0;k<36;k++){//k number of simulations
242     startvelocity(En[k],theta[k],phi[k],alpha,v);//calculation of starting
    ↪ velocity components
243     double yo[] = {rStart,0,zStart,v[0],v[1],v[2]};//starting array y =
    ↪ (r,v)
244     vector<double> y,dydx(6),yout(6);
245     for(int i = 0;i < 6;i++){
246         y.push_back(yo[i]);//starting components are red into vector element
247     }
248
249     std::stringstream filename;// filename for .dat file in which the
    ↪ simulated variables are written into
250     filename << En[k]*1000 << "_" << theta[k] << "_" << phi[k] <<
    ↪ "_fin_h16.dat";
251     string s;
252     filename >> s;
253
254     // v_par,v_nor velocity components parallel and perpendicular to the
    ↪ magnetic field
255     // B is the B-field strength
256     // Volt is the Voltage
257     // br,bz,er,ez variables for field values storage and later input into
    ↪ fielstream for data storage
258     double v_par,v_nor,B,Volt,br,bz,er,ez;
259
260     for(int n = 0; n < 5000;n++){
261         try{
262             // first get the derivative at the startpoint of the
    ↪ runge-kutta-step
263             derivs(y,dydx,ER,EZ,BR,BZ);
264             // readout of field values at startpoint for data storage
265             param(y,BR,BZ,V,v_par,v_nor,B,Volt,br,bz,er,ez,ER,EZ);
266             ofstream myfile;
267             myfile.open (s,ios::app);
268             // relevant variables are read into file
269             myfile << y[0] << " " << y[1] << " " << y[2] << " " << B << " "
    ↪ << br << " " << bz << " " << er << " " << ez << " " <<
    ↪ Volt;
270             myfile.scientific;

```



```

271 myfile.precision(13);
272 myfile << " " << v_nor << " " << v_par<< " " << y[3] << " " <<
    ↪ y[4] << " " << y[5] << "\n";
273 myfile.close();
274 // calculate current pinch angle
275 pinchangle =
    ↪ 180*acos(v_par/(sqrt(v_par*v_par+v_nor*v_nor)))/M_PI;
276 // interrupt simulation if the pinch angle is above 90°,
    ↪ because than the electron has been reflected
277 if(pinchangle > 90)break;
278 //interrupt simulation if the electron is out of bounds
279 if(y[2] < 0)break;
280 // calculate stepsize for the next runge-kutta-step
281 h = stepsize(16,y,BR,BZ);
282 // calculate next runge-kutta-step
283 rk4(y,dydx,h,yout,ER,EZ,BR,BZ);
284 // save current position
285 y = yout;
286 }catch(const out_of_range e){
287     cout << e.what()<<"\n";
288     break;
289 }
290 }
291 }
292 return 0;
293 }

```